04,08

Comparative crystal structure study of thin films of stoichiometric and non-stoichiometric titanium oxides

© A.K. Markelova, D.A. Kalmykov, V.A. Voronkovskii, V.Sh. Aliev , V.I. Vdovin, A.K. Gutakovskii

Rzhanov Institute of Semiconductor Physics, Siberian Branch, Russian Academy of Sciences, Novosibirsk, Russia

¶ E-mail: aliev@isp.nsc.ru

Received June 6, 2025 Revised June 20, 2025 Accepted June 22, 2025

The crystal structure of thin films of stoichiometric TiO_2 and non-stoichiometric $TiO_{2-\delta}$ ($\delta=0.9$) compositions, synthesized by ion beam sputtering deposition and annealed at temperatures of 723-973 K in argon atmosphere has been studied. It was found that the films of stoichiometric composition crystallize according to the dendritic growth mechanism at the initial stage. After the growth of dendrites before their interactions with each other, layered growth mechanism is observed with the formation of lamellar crystals. Films of non-stoichiometric composition crystallize according to the island growth mechanism. The activation energy of the crystallization front movement was determined for the dendritic growth mechanism, which was 2.3 eV. TiO_2 films after annealing consisted of plate-shaped crystals of rutile phase with inclusions of anatase nanocrystals. The films of non-stoichiometric composition were nano-dispersed, containing crystalline phases: anatase, rutile, α - Ti_3O_5 and α -Ti.

Keywords: thin films, titanium oxides, ion-beam sputtering-deposition, crystallization, HRTEM, SEM.

DOI: 10.61011/PSS.2025.06.61689.158-25

1. Introduction

Thin films of titanium oxides have a wide spectrum of electrophysical properties due to their structural diversity. They became widely used in various fields of science and engineering, for example as follows: a functional layer for resistive memory cells [1], a heat sensitive layer for microbolometric matrices [2], optical and bactericide coatings [3,4].

Films of non-stoichiometric composition $TiO_{2-\delta}$ (δ parameter of oxide composition deviation from stoichiometric one (TiO₂)) spark outstanding interest since the parameter δ radically impacts the optical [5,6] and electric properties of the films [7]. It is evident that the impact of the parameter δ on the electrophysical properties is the effect of structural and morphological transformation of non-stoichiometric films upon their crystallization, for Structural transformation asexample, after annealing. sumes transformation of an amorphous phase into various crystalline phases, and morphological one - formation of compounds from crystals having different geometric shapes, spatial orientation and dimensions. Despite the fact that thin films of titanium oxides, of both stoichiometric and nonstoichiometric compositions, are widely used for various applications, the literature contains practically no papers dedicated to the study of the parameter δ impact on their crystalline and morphological structure and on the crystallization mechanism.

Controlled and reproducible formation of thin titanium oxide films with the specified composition, crystalline structure and morphology is one of the material science problems of their use in microbolometers. Within this problem, the aim of this work is a comparative structural and morphological analysis of thin TiO_2 and $\text{TiO}_{2-\delta}$ ($\delta=0.9$) films during their annealing in pure argon atmosphere. Previously, we found that films with $0.11 < \delta \leq 1.0$ provided the best optical parameters suited for bolometers in the THz range of electromagnetic radiation [5]. Therefore, to compare structural and morphological differences, non-stoichiometric films with $\delta=0.9$ were chosen.

2. Film synthesis

For synthesis of films of non-stoichiometric titanium oxides $TiO_{2-\delta}$ ($\delta = 0.9$), the ion beam sputtering deposition method (IBSD) was used [8]. pressure in the vacuum chamber before the films deposition was 10^{-4} Pa. For sputtering, a titanium metal target was used (Ti > 99.92 %, BT1-00 grade, GOST 19807-91). The target was sputtered by Ar⁺ ions with an energy of 1200 eV. The ion flux density on the surface of the sputtered target was permanent and was equal to 1.0 mA/cm². To obtain oxides, high purity oxygen was supplied to the chamber $(O_2 > 99.999\%, TU 6-21-12-94, "SibTechGas"$ JSC). Various parameter δ values were set by changing the oxygen concentration in the vacuum chamber. Partial oxygen pressure in the film deposition area was varied in the range from $0.6 \cdot 10^{-3}$ to $1.0 \cdot 10^{-2}$ Pa with precision of $(\pm 10\%).$

Substrates used were KEF-4.5 Si(100) wafers with a thermal SiO₂ layer (100 nm thick). The substrates temperature during film deposition did not exceed 350 K. The film thickness was controlled by a quartz crystal microbalance (Maxtek, Inc.). According to the quartz

4 929

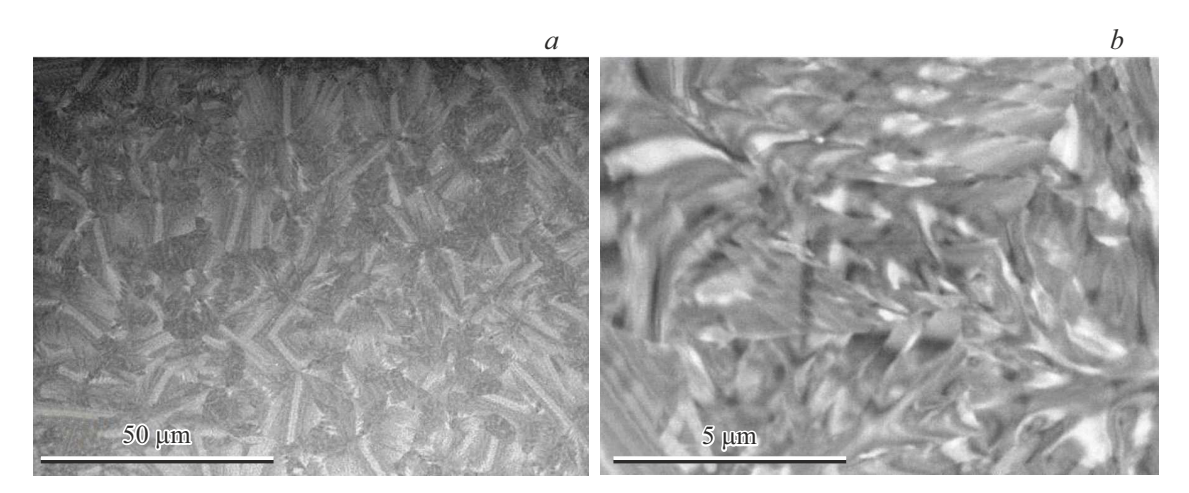


Figure 1. SEM images of the stoichiometric TiO₂ film crystalline structure after annealing in the argon atmosphere at 973 K for 20 min at different magnifications.

sensor, the deposition rate was around 0.08 nm/s. According to ellipsometry, the typical film thickness was about 50 nm.

The deposited films were annealed at different temperatures from 673 to 973 K in the argon atmosphere. It has been experimentally established that the argon purity during annealing of films substantially affects their morphology. Therefore, the experiments used high purity argon (oxygen-containing impurities < 0.001%, TU 20.11.11-001-06069174-2017, "PromGas" LLC). For annealing, a quartz furnace with optical chamber heating was used.

3. Research methods

Structural studies were made using a scanning electron microscope (SEM) Hitachi SU8220 and a high-resolution transmission electron microscope (HRTEM) TITAN 80-300 (FEI) equipped with an objective lens spherical aberration corrector and an energy-dispersive X-ray spectrometer (EDX). Digital processing of experimental images produced by the HRTEM method was carried out using the commercial microscopy suite software GATAN (GMS-3.5) and included formation of fast Fourier transform (FFT) patterns. FFT patterns were used to better visualize the atomic structure of certain crystals in the films and to establish their crystalline structure parameters.

To obtain HRTEM images, at first, free-hanging membranes of thermal SiO_2 with a $3-8\,\mu m$ thick silicon sublayer were prepared. The membranes were prepared by the method of local deep anisotropic etching of $Si(100)/SiO_2$ silicon substrate in 20% aqueous solution of tetramethyl ammonia hydroxide with visual control of residual silicon thickness by the membrane color in the light. Then TiO_2 or $TiO_{2-\delta}$ films were deposited on the membranes for the study. One part of the films on the membranes was annealed, whereas the other was not. Prior to the films study utilizing the HRTEM method, the silicon sublayer and, partially, the SiO_2 film were removed in a plasma-chemical reactor with SF_6 etching gas.

4. Experimental results

4.1. Structure and composition of virgin non-annealed films

Grown films of stoichiometric composition were amorphous, contrary to the films of non-stoichiometric composition, the amorphous phase of which contained inclusions of nanocrystals less that 10 nm in size. Nanocrystals had tetragonal crystalline lattice and corresponded to the TiO composition, according to the article [9].

The chemical composition of the films was previously established by us using the X-Ray photoelectron spectroscopy (XPS) method [5]. The dependence between the parameter δ and the partial oxygen pressure in the film growth area was determined. This dependence made it possible for us to obtain the parameter δ of grown $\text{TiO}_{2-\delta}$ films using the partial oxygen pressure without resorting to the XPS measurements.

4.2. Structure of films of stoichiometric composition

After annealing of 50 nm thick amorphous stoichiometric films, crystals of different shapes and sizes were formed. Figure 1 shows the examples of plate-shaped crystals distributed in the entire thickness of the film. In addition, bulk-type nanocrystals were observed (Figure 2, a). To confirm that the nanocrystals were titanium oxides, EDX spectra were recorded (Figure 2, b). It was verified that Si peak in the EDX spectrum is related to the residual SiO₂ membrane layer. According to the HRTEM image and the FFT pattern analysis, anatase and rutile phases were observed in the film (Figure 3). Most of the HRTEM image area (Figure 3) corresponded to the rutile phase, and inclusions outlined with white oval lines in the figure, corresponded to the anatase phase. The island shape of inclusions indicates the three-dimensional mechanism of their nucleation and growth [10].

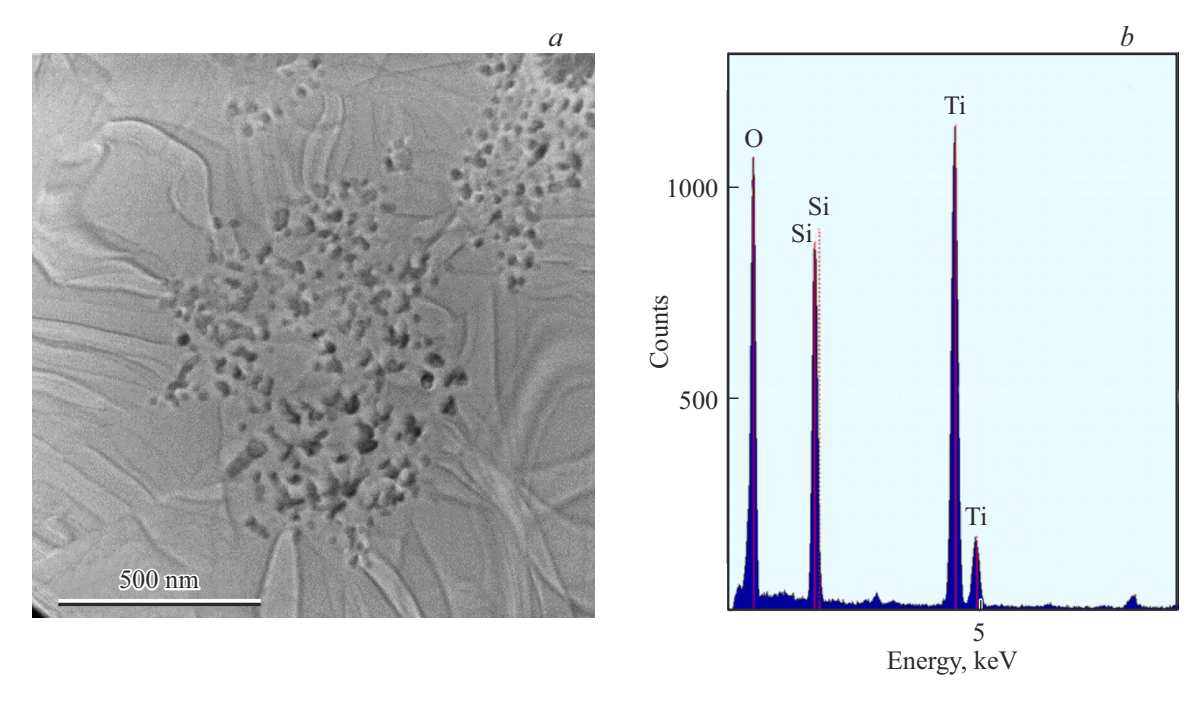


Figure 2. HRTEM image of the stoichiometric TiO_2 film crystalline structure after annealing in the argon atmosphere at 973 K for $20 \min (a)$ and the corresponding EDX spectrum (b).

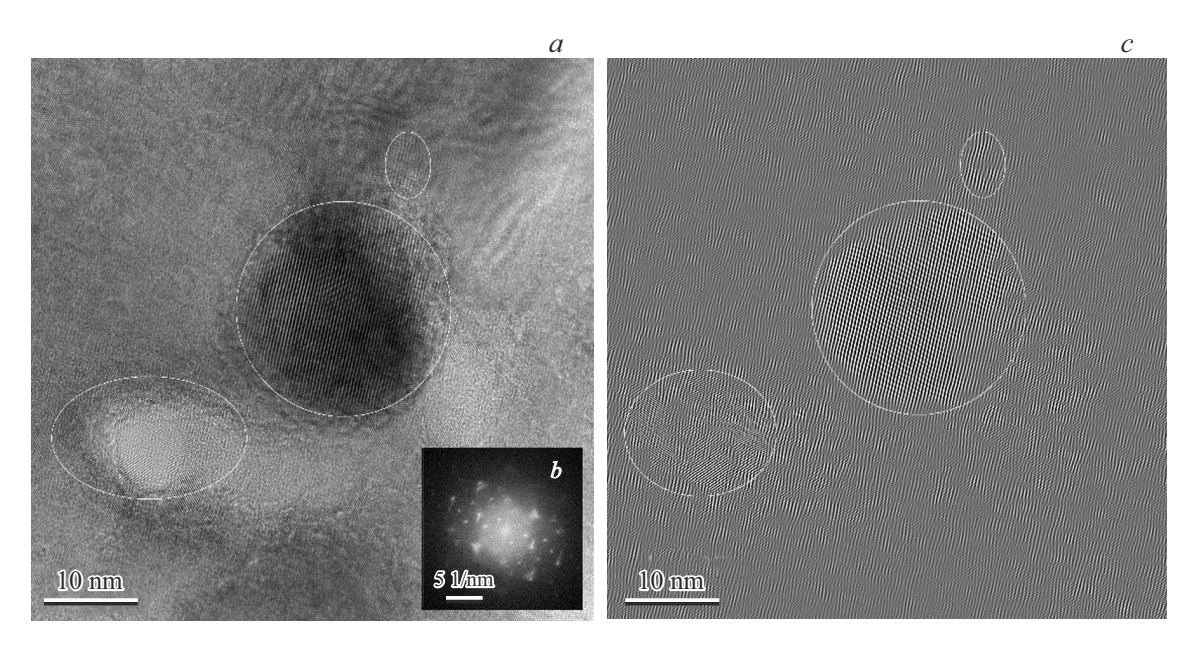


Figure 3. HRTEM image of the annealed TiO_2 film fragment (a), the corresponding FFT pattern (b) and the HRTEM image filtered by anatase diffraction reflexes (c).

4.3. Structure of films of non-stoichiometric composition

The film of non-stoichiometric composition after annealing had a closely-packed fine-dispersed polycrystalline structure with nanocrystals approximately 20 nm in size (Figure 4).

Nanocrystals of the anatase phase filled most of the HRTEM image area (Figure 4, b). In addition, the following

phases were observed: rutile phase, Ti_3O_5 phase, and metal α -Ti phase (Figure 5).

4.4. Crystallization kinetics

During annealing of titanium oxide films of stoichiometric composition, plate-shaped microcrystals larger than $10\,\mu m$ were observed, contrary to the films of non-stoichiometric composition with nanoscale crystals. Such large dimensions

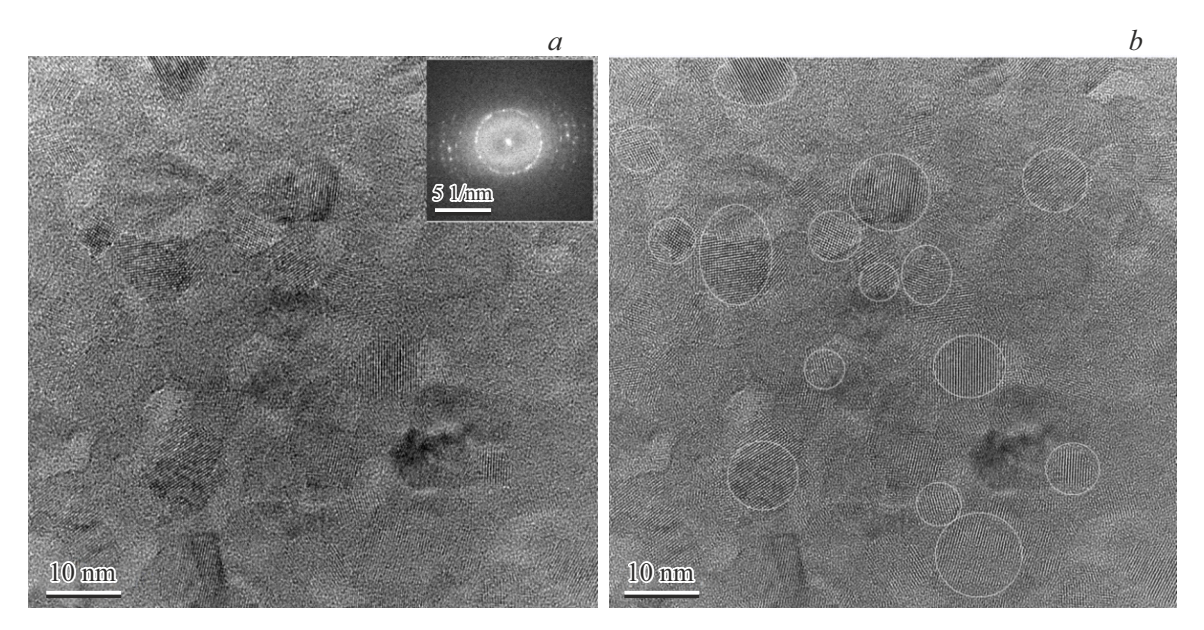


Figure 4. HRTEM image of the non-stoichiometric film after annealing (a) and the image filtered by anatase phase reflexes (b). Anatase phase contours are outlined with white lines. The inset in (a) shows the FFT pattern.

of crystals in TiO_2 films made it possible to track the initial stage of crystallization by the SEM method (Figure 6). It can be seen that microcrystals were flat and round in shape. The microcrystal morphology indicates the dendritic growth nature in the conditions of constrained crystallization. The number of microcrystals and their average dimensions depended on the annealing temperature. As the annealing temperature decreased, so did the diameters of microcrystals and their concentration (Figure 7).

5. Discussion

According to the article [11], there are several crystallization mechanisms: the layer, island and dendritic ones. For stoichiometric titanium oxides, the dendritic crystallization was observed initially. Once the dendrites had grown to a size where they started interacting with each other, the layer growth mechanism was observed, leading to the formation of plate-like crystals. For non-stoichiometric oxides, the island crystallization mechanism was observed. In the first case, the crystalline phase was formed in a thin nearsurface layer. Additionally, the chemical composition of the crystalline phase was the same as that in the amorphous The velocity of crystallization front movement parallel to the film surface was much higher than that along the surface normal. As a result, layers were formed, which consisted of plate-shaped crystals with dimensions reaching dozens of microns in the lateral direction and clearly visible using the SEM method. In the second case, a fine-dispersed polycrystalline film was formed, which consisted of nanocrystals with varying chemical composition and structure.

During annealing of amorphous TiO_2 films after formation of the crystalline phase nucleus in sites of potential condensation of oxygen vacancies, this nucleus grew to a size comparable to the film thickness (50 nm). Simultaneously, the nanocrystal growth occurred in the lateral direction along the film surface. It is important to note that the lateral growth at the initial stage occurred in an isotropic manner in all directions along the surface, therefore microcrystals were round and disc-shaped (Figure 6).

The SEM images (Figure 7), captured for the films annealed at different temperatures, made it possible to assess the activation energy for the disc growth process. The disc growth process can be characterized by the crystallization front velocity (η) along the film surface. Obviously, $\eta = \partial r/\partial t$, where: r—disc radius, t—current time of growth process. Disc radii in the film differed, which indicated the random nature of crystalline phase nuclei appearance during the annealing process. It follows then that the radius of random ith disc at the moment of time t after the start of annealing was equal to:

$$r_i(t) = \xi(\tau_i)\eta(t - \tau_i), \tag{1}$$

where

$$\xi(\tau_i) = \begin{cases} 0, & t < \tau_i \\ 1, & t \ge \tau_i \end{cases}$$

 τ_i — the moment of formation of the *i*th nucleus of the disc-shaped crystalline phase.

The total area of discs (S) per unit of film surface area at the initial stage of crystallization is of interest, since this value can be determined experimentally. The S value growth speed is determined by the total length of disc

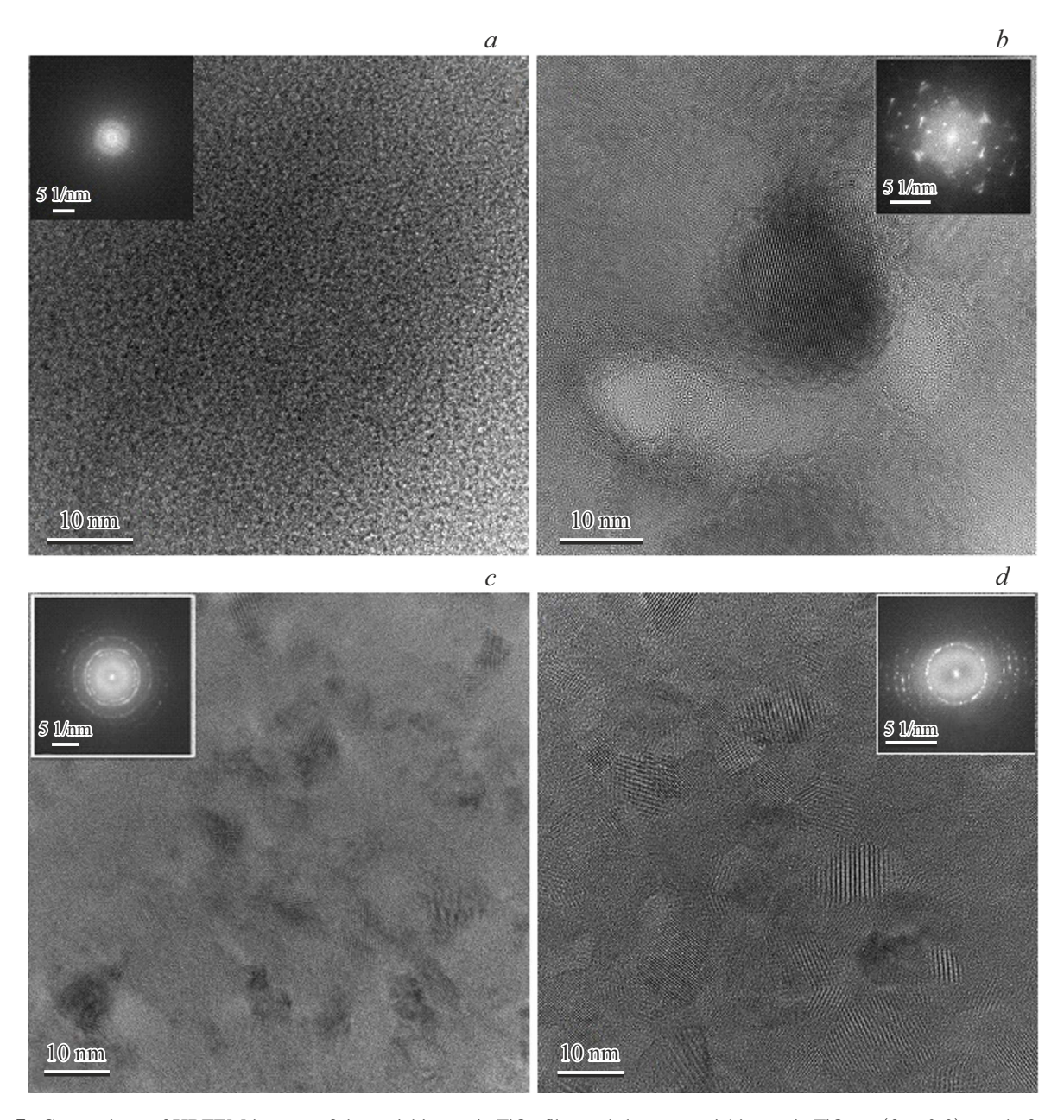


Figure 5. Comparison of HRTEM images of the stoichiometric TiO_2 film and the non-stoichiometric $\text{TiO}_{2-\delta}$ ($\delta=0.9$) one before (a and c, respectively) and after annealing at 973 K for 20 min (b and d, respectively). The insets show the corresponding FFT patterns.

circumferences and crystallization front velocity:

$$\frac{\partial S}{\partial t} = 2\pi \eta \sum_{i=1}^{n} r_i(t), \tag{2}$$

where n — number of discs per unit of film area at the moment of time t. Integration of equation (2) taking into account (1), provides the S value during film crystallization for t_0 :

$$S(t_0) = 2\pi \eta^2 \int_0^{t_0} \left[\sum_{i=1}^n \xi(\tau_i)(t - \tau_i) \right] dt.$$
 (3)

The $S(t_0)$ value is a function of random τ_i and n values. The average $S(t_0)$ value was determined experimentally from the film SEM images. For this, the $S(t_0)$ value was measured for five random sections of the SEM image of the film and then averaged. After that, the average $S(t_0)$ values were determined for various annealing temperatures (Figure 7).

The integral in equation (3) is practically independent of the temperature in the range of T = 723-773 K, assuming that the average n value is limited to concentration of oxygen vacancies in amorphous TiO_2 film and is determined only by the annealing time t_0 . These values, concentration of oxygen vacancies and annealing time, were the same for all

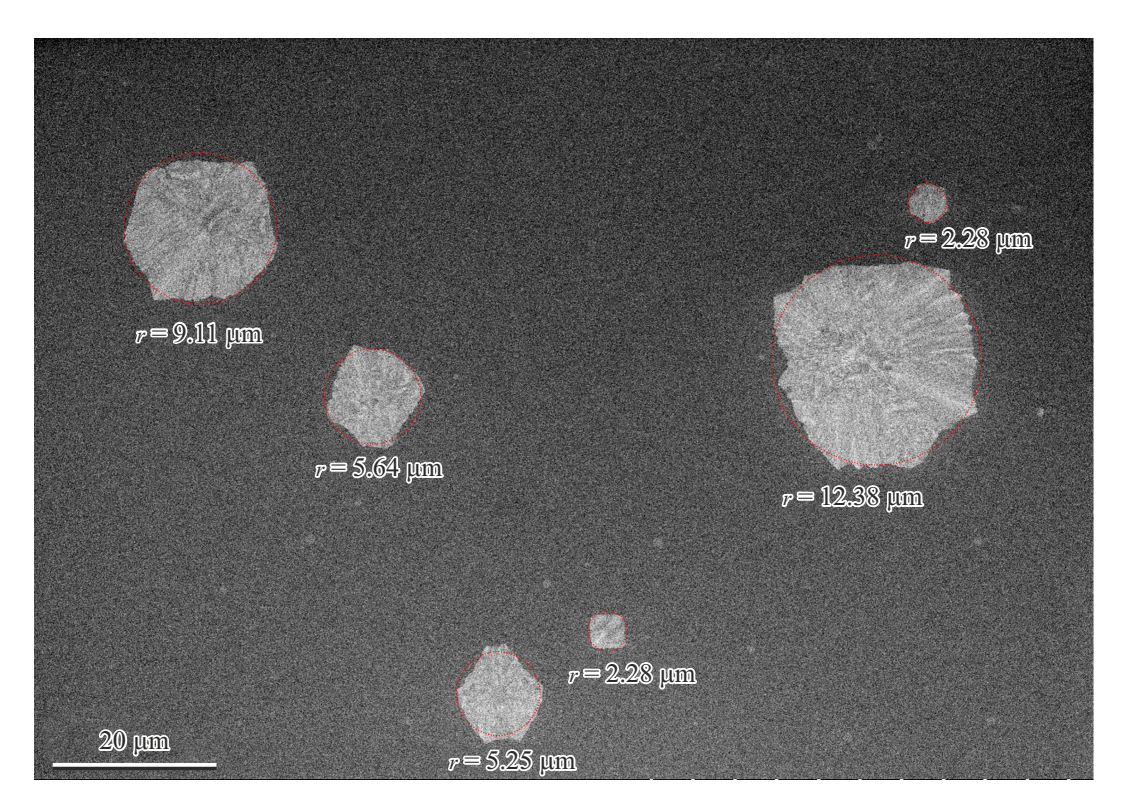


Figure 6. SEM image of the thin TiO_2 film after annealing in the argon atmosphere at 753 K for 20 min. Microcrystals are circled in red (red dotted lines) specifying their radii (r).

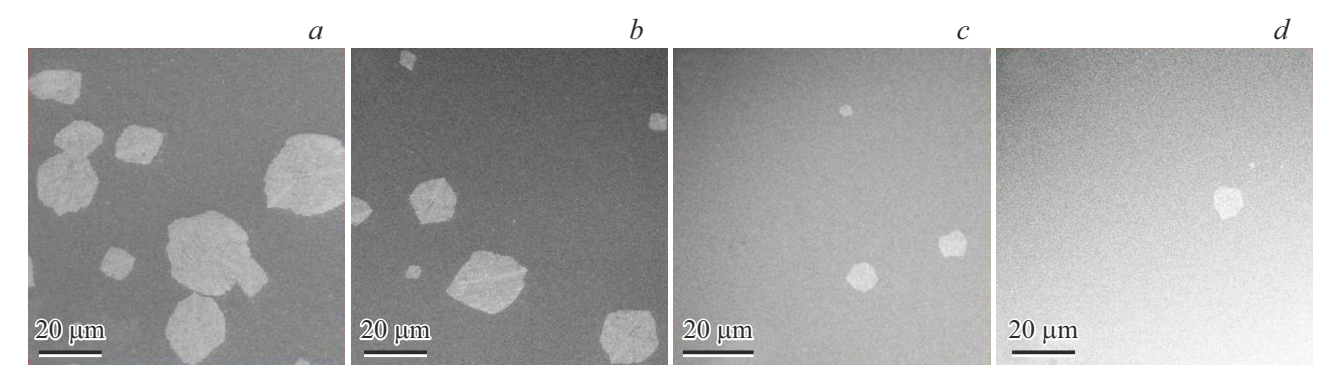


Figure 7. SEM images of the thin TiO_2 film after annealing in the argon atmosphere at different temperatures for 20 min: a - 773 K, b - 763 K, c - 743 K and d - 723 K.

films. Therefore, temperature dependence of the average $S(t_0)$ value was determined by temperature dependence of the η^2 value. Therefore, the crystallization front movement velocity η is proportionate to the following:

$$\eta \propto \sqrt{S(t_0)}$$
.

Temperature dependence of the η value, plotted in the Arrhenius form, is shown in Figure 8. One can see that all experimental points can be fitted by one straight line, and the activation energy of crystallization front movement was around 2.3 eV.

Description of crystallization in a thin layer is complicated by the presence of two heteroboundaries and the presence of mechanical stresses, developed by the substrate when heated and cooled during the annealing process. Therefore, the suggested description of the flat disc growth does not attempt to describe the kinetics of crystalline phase formation from amorphous matrix, as it is done, for example, in the book [12]. In this paper, the activation energy of the limiting stage of disc-shaped crystal growth was determined experimentally assessing the value of disc area in the thin layer using the SEM images. The question remains open as to which process at the atomic level the found activation energy value corresponds to.

For non-stoichiometric titanium oxides, the island crystallization was observed during the annealing process. The

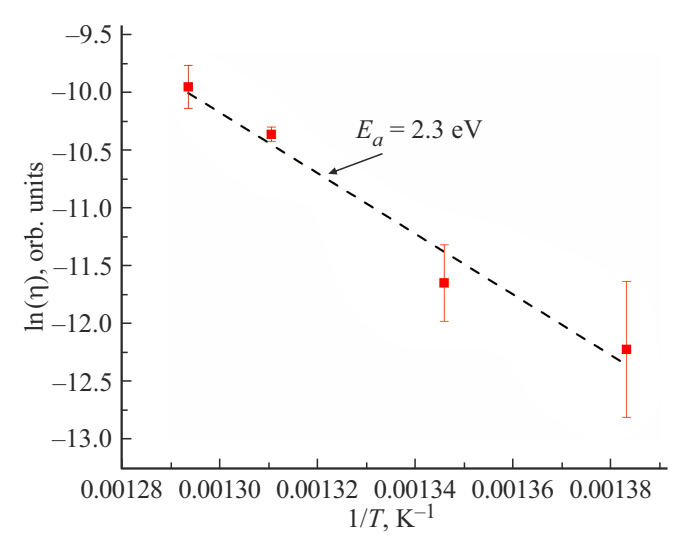


Figure 8. Crystallization front velocity η dependence on annealing temperature T. E_a — activation energy of crystallization front movement.

films after annealing were fine-dispersed and polycrys-It is interesting to compare the structural and morphological changes in the films of stoichiometric and non-stoichiometric compositions before and after annealing (Figure 5). The type of FFT patterns depends on the film crystallinity, mutual orientation of crystals and crystal dimensions. Amorphousness of the virgin films of stoichiometric composition was confirmed by the FFT pattern shown in Figure 5, a. Large plate-shaped microcrystals in the annealed films of stoichiometric composition, contrary to the non-stoichiometric composition, formed the dotted FFT pattern (Figure 5, b). In the non-annealed films of non-stoichiometric composition, the group of randomly disoriented nanocrystals formed a FFT pattern in the form of circumferences (Figure 5, c). This indicates that before annealing, during the film deposition process, the nanocrystals originated independently from each other, and their dimensions were substantially smaller than the film thickness. It is obvious that after annealing the nanocrystals grew and started interacting with each other. In addition, their growth was limited by the film thickness, which caused a certain growth direction, i.e. texture formation. As a result, the FFT pattern transformed from a set of circumferences into a set of arcs (Figure 5, d).

Radical difference of morphology in crystalline phases of stoichiometric and non-stoichiometric films of titanium oxide, in our opinion, is related, first of all, to the concentration of crystallization centers formed during the annealing process of amorphous films. The crystallization centers were volumetric defects formed from the aggregates of oxygen vacancies. It is known that the concentration of oxygen vacancies is directly related to the chemical composition of films and may reach several dozens of atomic percents [13]. On the other hand, as shown in the article [13], the combination of oxygen vacancies into

divacancies in titanium oxides is energetically beneficial. Divacancies, contrary to vacancies, have high mobility in solids, which promotes their active participation in the structural and morphological transformation of the film [14]. The results that we obtained confirmed the decisive role of oxygen vacancies in the formation of structure and morphology of thin titanium oxide films. Indeed, since the density of vacancies in the non-stoichiometric $TiO_{2-\delta}$ ($\delta = 0.9$) oxide was much higher than that in the stoichiometric TiO₂ oxide, then, correspondingly, there were much more crystallization centers. When $TiO_{2-\delta}$ films were annealed, the nanocrystals limited the growth of each other. Therefore, the nano-dispersed crystalline structures were formed in the films of non-stoichiometric compositions of oxides by annealing (Figure 4), and plate crystals of micron size were formed in the films of stoichiometric oxides, where there were much less crystallization centers (Figure 1). On the other hand, the aggregates of oxygen vacancies in non-stoichiometric oxides formed the crystallization centers, the chemical composition of which differed from anatase and rutile, which caused diversity of phase composition of titanium oxides in the annealed films.

6. Conclusion

In this paper it is demonstrated that the structure and morphology of the crystalline phase of titanium oxide films radically depends on the stoichiometric composition of virgin amorphous $\text{TiO}_{2-\delta}$ films. The parameter δ specifies, first of all, the concentration of crystallization centers, and, correspondingly, the crystalline phase morphology. Secondly, the parameter δ specifies the chemical composition and structure of crystallization centers, which determines the phase composition of crystals in the film after annealing.

The found activation energy value for the growth of discshaped crystals may turn out to be useful for the researchers involved in modeling of the crystallization process in thin films, to compare the results of their calculations with the experiment. In this regard, for unambiguous interpretation of the experimental result, the terminology and assumptions of (formulae (1)-(3)) were described, which produced the activation energy value.

Obviously, the morphology and the structure of crystalline phases have a substantial effect on the electroconductivity of the films, which is critical for their practical use. For example, the fine-dispersed titanium oxide films, which consist of conducting clusters in a dielectric matrix, are the most suitable for use in bolometers. Such films may be formed using non-stoichiometric titanium oxide films. In accordance with the results of this paper, the primary role for reproducible formation of thin titanium oxide films is played by the control of their stoichiometry.

Acknowledgments

The authors express their gratitude to the employee of the Institute of Semiconductor Physics, Siberian Branch of the Russian Academy of Sciences, Yu.A. Zhivodkov for the specimen analysis by SEM method ("Nanostructures" Collective Use Center, ISP SB RAS).

Funding

This study was supported by the Russian Science Foundation under project No. 24-29-00344. HRTEM studies were performed on equipment of the "Nanostructures" Collective Use Center with the support of the Russian Science Foundation project No. 19-72-30023.

Conflict of interest

The authors declare that they have no conflict of interest.

References

- J.J. Yang, M.D. Pickett, X. Li, D.A. Ohlberg, D.R. Stewart, R.S. Williams. Nature nanotechnology 3, 7, 429 (2008). DOI: 10.1038/nnano.2008.160
- [2] Y.J. Jeong, S.G. Kang, M.H. Kwon, H. Jung. Proc. SPIE 10624, Infrared Technology and Applications XLIV, 106241F (31 May, 2018). DOI: 10.1117/12.2309764
- [3] V.V. Atuchin, V.N. Kruchinin, A.V. Kalinkin, V.Sh. Aliev, S.V. Rykhlitsky, V.A. Shvets, E.V. Spesivtsev. Optika i spektroskopiya **106**, *1*, 77 (2009). (in Russian).
- [4] A.A. Goncharov, A.N. Dobrovolsky, E.G. Kostin, I.S. Petrik, E.K. Frolova. ZhTF 84, 6, 98 (2014). (in Russian). https://journals.ioffe.ru/articles/viewPDF/27261
- [5] A.K. Gerasimova, V.A. Voronkovsky, D.A. Kalmykov, V.Sh. Aliev, V.A. Volodin, M.A. Demianenko. Optika i spektroskopiya 133, *I*, 57 (2025). (in Russian). DOI: 10.61011/OS.2025.01.59880.7201-24
- [6] S.V. Bulyarsky, D.A. Koiva, G.G. Gusarov, V.V. Svetukhin. Optika i spektroskopiya 129, 11, 1426 (2021). (in Russian). DOI: 10.21883/OS.2021.11.51645.2428-21
- [7] M. Niu, H. Tan, D. Cheng, Z. Sun, D. Cao. J. Chem. Phys. 143, 5, 054701 (2015). DOI: 10.1063/1.4928062
- [8] V.A. Shvets, V.Sh. Aliev, D.V. Gritsenko, S.S. Shaimeev, E.V. Fedosenko, S.V. Rykhlitski, V.V. Atuchin, V.A. Gritsenko, V.M. Tapilin, H. Wong. J. Non-Cryst. Solids 354, 3025 (2008). DOI: 10.1016/j.jnoncrysol.2007. 12. 013
- [9] D. Watanabe, J.R. Castles, A. Jostsons, A.S. Malin. Acta Crystallogr. 23, 2, 307 (1967).
- [10] E. Baldini, L. Chiodo, A. Dominguez, M. Palummo, S. Moser, M. Yazdi-Rizi, M. Chergui. Nat. Commun. 8, 1, 13 (2017). DOI: 10.1038/s41467-017-00016-6
- [11] A.G. Bagmut. Pisma v ZhTF 38, 10, 79 (2012). (in Russian).
- [12] L.N. Aleksandrov. Kinetika obrazovaniya i struktura tverdykh sloev. Iz-vo Nauka, Sibirskoe otdelenie, Novosibirsk (1972). S. 11. (in Russian).
- [13] A.A. Rempel, A.I. Gusev. Nestekhiometriya v tverdom tele. Fizmatlit, M. (2018). S. 118. (in Russian).
- [14] D.A.H. Hanaor, C.C. Sorrell. J. Mater. Sci. 46, 855 (2011). DOI: 10.1007/s10853-010-5113-0

Translated by M.Verenikina